J|A|C|S
ARTICLES
Published on Web 03/22/2002

Reaction Path Analysis of the "Tunable" Photoisomerization Selectivity of Free and Locked Retinal Chromophores

Luca De Vico,[†] Christopher S. Page,[†] Marco Garavelli,*[,§] Fernando Bernardi,[§] Riccardo Basosi,[†,‡] and Massimo Olivucci*[,†,‡]

Contribution from the Dipartimento di Chimica, Università di Siena, via Aldo Moro, Siena, I-53100 Italy, Centro per lo Studio dei Sistemi Complessi, Via Tommaso Pendola 37, Siena I-53100 Italy, and Dipartimento di Chimica "G. Ciamician", Università di Bologna, via Selmi 2, Bologna, I-40126 Italy

Received November 9, 2001

Abstract: Multiconfigurational second-order perturbation theory computations and reaction path mapping for the retinal protonated Schiff base models all-*trans*-nona-2,4,6,8-tetraeniminium and 2-*cis*-nona-2,4,6,8-tetraeniminium cation demonstrate that, in isolated conditions, retinal chromophores exhibit at least three competing excited-state double bond isomerization paths. These paths are associated with the photoisomerization of the double bonds in positions 9, 11, and 13, respectively, and are controlled by barriers that favor the position 11. The computations provide a basis for the understanding of the observed excited-state lifetime in both naturally occurring and synthetic chromophores in solution and, tentatively, in the protein environment. In particular, we provide a rationalization of the excited-state lifetimes observed for a group of locked retinal chromophores which suggests that photoisomerization in bacteriorhodopsin is the result of simultaneous specific "catalysis" (all-trans → 13-cis path) accompanied by specific "inhibition" (all-trans → 11-cis path). The nature of the $S_1 \rightarrow S_0$ decay channel associated with the three paths has also been investigated at the CASSCF level of theory. It is shown that the energy surfaces in the vicinity of the conical intersection for the photoisomerization about the central double bond of retinal (position 11) and the two corresponding lateral double bonds (positions 9 and 13) are structurally different.

1. Introduction

The protonated Schiff base of retinal (PSB) is the chromophore of rhodopsin proteins.[1−5] These include the retina visual pigment of superior animals (rhodopsin), the proton and chloride pumping pigments of *Halobacterium halobium* (bacteriorhodpsin and halorhodopsin, respectively), and other bacterial light sensing pigments (sensory rhodopsins). The biological activity of rhodopsins is triggered by the light-induced cis−trans isomerization of the corresponding chromophores that, in turn, induces a conformational change in the protein.

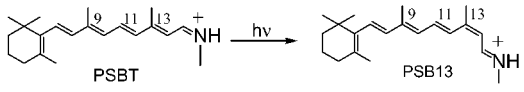

(1)

Native PSB chromophores occur in different stereoisomeric forms such as all-trans in bacteriorhodopsin and sensory rhodopsins, 11-cis in rhodopsin, 13-cis in the dark-adapted bacteriorhodopsin,[1−5] and 9-cis in the artificial pigment isorhodopsin.[6,7] Despite these stereochemical differences, the photoisomerization of PSBs *in the protein cavity* is stereospecific. This means that, upon irradiation, only one PSB stereoisomer is generated from the initial form. For instance, in bacteriorhodopsin, the all-trans PSB (PSBT) chromophore yields the 13-cis PSB form (PSB13) exclusively. This behavior is in contrast to the result of PSBT irradiation *in solution*, where a mixture of different isomers (i.e., 17% 13-cis, 64% 11-cis, and 10% 9-cis) is produced, and the stereospecificity is lost.[8] Furthermore, while PSB13 is the only photoproduct of bacteriorhodopsin photolysis, the major product of PSBT photolysis in solution is the 11-cis form (PSB11).[8] It is therefore apparent that the protein environment is able to "catalyze" the PSBT → PSB13 reaction with respect to alternative PSBT → PSB11 and PSBT → PSB9 processes.

The lack of stereospecificity observed in solution suggests that competitive or nearly competitive excited-state reaction paths exist in the isolated PSB chromophores that correspond

* To whom correspondence should be addressed. E-mail: M.G., mgara@ciam.unibo.it; M.O., olivucci@unisi.it.
† Università di Siena.
‡ Centro per lo Studio dei Sistemi Complessi.
§ Università di Bologna.

(1) Mathies, R. A.; Lugtenburg, J. In *Handbook of Biological Physics*; Stavenga, D. G., De Grip, W. J., Pugh, E. N., Eds.; Elsevier Science: New York, 2000; Vol. 3.
(2) Needleman, R. In *CRC Handbook of Organic Photochemistry and Photobiology*; Horspool, W. M., Song, P.-S., Eds.; CRC Press: Boca Raton, FL, 1995.
(3) Ottolenghi, M.; Sheves, M. *Isr. J. Chem.* **1995**, *35*, 193−513.
(4) Wald, G. *Science* **1968**, *162*, 230−239.
(5) Yoshizawa, T.; Kuwata, O. In *CRC Handbook of Organic Photochemistry and Photobiology*; Horspool, W. M., Song, P.-S., Eds.; CRC Press: Boca Raton, FL, 1995.
(6) Hurley, J. B.; Ebrey, T. G.; Honig, B.; Ottolenghi, M. *Nature (London)* **1977**, *270*, 540−542.
(7) Liu, R. S. H.; Crescitelli, F.; Denny, M.; Matsumoto, H.; Asato, A. E. *Biochemistry* **1986**, *25*, 7026−7030.
(8) Freedman, K. A.; Becker, R. S. *J. Am. Chem. Soc.* **1986**, *108*, 1245−1251.

10.1021/ja017502c CCC: $22.00

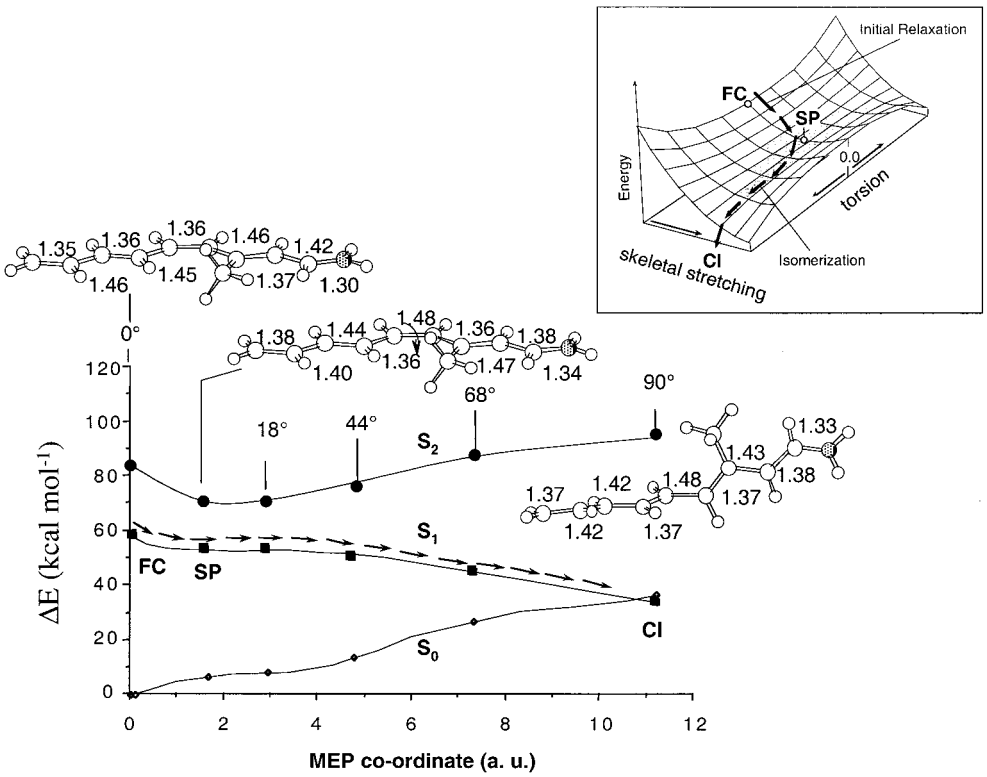

Figure 1. Energy profiles along the S_1 11-cis → all-trans photoisomerization coordinate of **1**. The structures (geometrical parameters in Å and deg) document the progression of the molecular structure along the coordinate (data are from ref 9). Full squares indicate the S_1 energies; full circles and diamonds indicate the S_2 and S_0 energies. The two-mode structure (stretching + torsion) of the S_1 reaction coordinate is illustrated in the inset. FC is the Franck−Condon structure, SP corresponds to the relaxed planar species, and CI is the 90° twisted S_1/S_0 conical intersection decay channel.

to torsional deformation about different double bonds (e.g., the double bonds in positions 9, 11, and 13). To support this hypothesis, we have carried out excited-state reaction path computations for different realistic PSB models in isolated conditions and in the absence of a counterion.

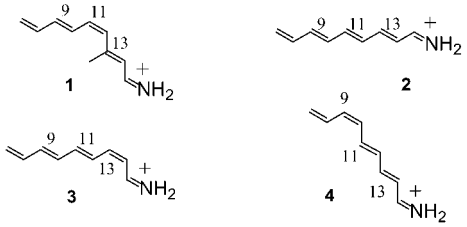

Recently we have reported the results of a series of ab initio multiconfigurational second-order perturbation theory computations on the PSB11 model 4-cis-γ-methylnona-2,4,6,8-tetraeniminium cation **1**.[9,10] This model has been validated by computing the absorption and fluorescence maxima, the change in dipole moment, and by simulating the resonance Raman spectra of PSB11 and its ^{13}C isotopomers in solution.[11] The computed data compare well with the corresponding experimental quantity suggesting that the terminal double bond of PSB11, which is part of the β-ionone ring, does not conjugate effectively with the remaining part of the π-system in the ground-state equilibrium geometry. This conclusion is supported by the twisted conformation of the β-ionone ring recently computed[12] and observed in the X-ray structure of rhodopsin.[13] On the other hand, upon excited-state relaxation, the change in bond order may lead to β-ionone planarization. This effect cannot be described with models **1** and **2**, but is currently under investigation in our laboratory. In analogy with model **1**, in the present work we use the all-*trans*-nona-2,4,6,8-tetraeniminium cation **2**, the 2-*cis*-nona-2,4,6,8-tetraeniminium cation **3**, and the 6-*cis*-nona-2,4,6,8-tetraeniminium cation **4** as PSBT, PSB13, and PSB9 models, respectively.

Photoisomerization path computations for **1** (see Figure 1) have demonstrated that the S_1 reaction coordinate (S_1 corresponds to the one B_u-like − hole-pair − spectroscopic state) is sequentially dominated by two substantially uncoupled modes.[10] As shown in the inset, the first mode is totally symmetric and drives the initially planar system out of the Franck−Condon point (FC) through a concerted double-bond stretch and single-bond compression. The second mode is asymmetric and is dominated by a cis−trans isomerization motion that is thus initiated only after the initial relaxation has produced a flat energy minimum (SP) where the central double bonds are stretched. The following evolution along the torsional coordinate leads to a conical intersection funnel (CI) where the chromophore displays a ca. 90° twisted central double bond and where, finally, fully efficient decay to the ground state occurs. Because the SP structure is planar, the FC → SP part of the path must be common to all possible isomerizations. Thus, in the following

(9) Garavelli, M.; Vreven, T.; Celani, P.; Bernardi, F.; Robb, M. A.; Olivucci, M. *J. Am. Chem. Soc.* **1998**, *120*, 1285−1288.
(10) Gonzalez-Luque, R.; Garavelli, M.; Bernardi, F.; Merchan, M.; Robb, M. A.; Olivucci, M. *Proc. Natl. Acad. Sci. U.S.A.* **2000**, *97*, 9379−9384.
(11) Garavelli, M.; Negri, F.; Olivucci, M. *J. Am. Chem. Soc.* **1999**, *121*, 1023−1029.
(12) Bifone, A.; de Groot, H. J. M.; Buda, F. *Chem. Phys. Lett.* **1996**, *248*, 165−172.
(13) Palczewski, K.; Kumasaka, T.; Hori, T.; Behnke, C. A.; Motoshima, H.; Fox, B. A.; Trong, I. Le; Teller, D. C.; Okada, T.; Stenkamp, R. E.; Yamamoto, M.; Miyano, M. *Science* **2000**, *289*, 739.

we present the results of a series of reaction path computations that document, for models **2**, **3**, and **4**, different SP → CI routes.

The excited-state dynamics of rhodopsin and bacteriorhodopsin have been recently investigated by carrying out time-resolved spectroscopic studies on artificial pigments where the natural PSB chromophores have been substituted with synthetic *locked* chromophores (see, for instance, the structures below).[14−17] In locked chromophores the torsional deformation of the reactive double bond (e.g., the double bond 11 in rhodopsin and the double bond 13 in bacteriorhodopsin) is prevented since the double bond is part of a cyclopentene moiety (see structures PSB13.5 and PSB11.5).

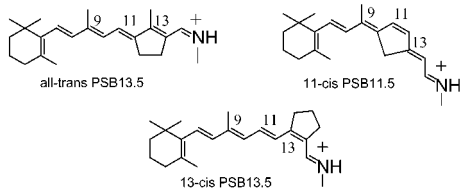

By using the all-trans PSB13.5 chromophore, Ottolenghi, Ruhman, Sheves, Atkinson, and co-workers[16] demonstrated that the time scale (less than 50 fs) of the initial excited-state dynamics of bacteriorhodopsin (i.e., the time scale for formation of a transient relaxed S_1 species) is not sensitive to the presence of the lock. On the basis of this experiment, the authors concluded, in agreement with the two-mode reaction coordinate of Figure 1, that the initial excited-state relaxation cannot be dominated by the all-trans → 13-cis isomerization motion. In further agreement with a two-mode model, the same experiment revealed that the rate of decay of such transients is very sensitive to the locking. In fact, while the excited state of native bacteriorhodopsin has a ca. 200 fs lifetime (with a product appearance time of 500 fs), the artificial pigment has a ca. 15 ps lifetime, thus indicating that all-trans → 13-cis motion must be involved in the excited-state decay. On the other hand, it must be stressed that a 15 ps lifetime still corresponds to a fast decay rate. This raises the problem of defining the nature of the radiationless decay channel operative in *locked* retinal proteins. Thus, in the present work we also present the results of excited-state reaction path computations for the locked PSB models **1-locked**, **2-locked**, and **3-locked**.

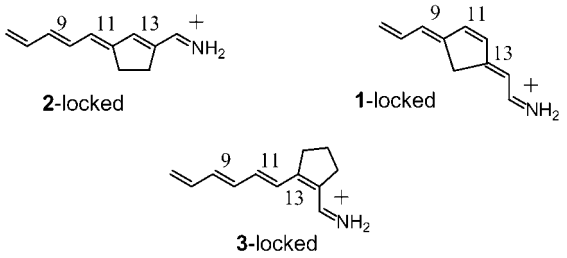

2. Computational Details

The molecular structures defining the SP → CI reaction coordinates for the **2**, **3**, **1-locked**, **2-locked**, and **3-locked** cations have been obtained via fully unconstrained geometry optimization and minimum energy path (MEP) computations using the complete active space self-consistent field (CASSCF) level of theory with the 6-31G* basis set. The procedure adopted to carry out these computations is reported in refs 18 and 19. In all cases, progression along the MEP is meausured in mass-weighted Cartesians (au = $amu^{1/2}a_0$). These computations have been carried out with the GAUSSIAN98 series of programs.[20] An active space of 10 electrons in 10 π-orbitals (10e/10o) has been used in all calculations. A two root (S_0, S_1) state average procedure was also used to avoid CASSCF convergence problems. To improve the reaction path energetics, we have performed single-point multiconfigurational second-order perturbation theory computations along a selected number of MEP points by using the CASPT2 method[21] included in MOLCAS-4.[22] The zeroth order wave functions used in the CASPT2 calculation are three root (S_0, S_1, and S_2) state average 10e/10o CASSCF wave functions. The S_0, S_1 CASSCF and S_0, S_1, and S_2 CASPT2 energy profiles for the all-trans → 11-cis isomerization of model **2** are given in Figure 2.

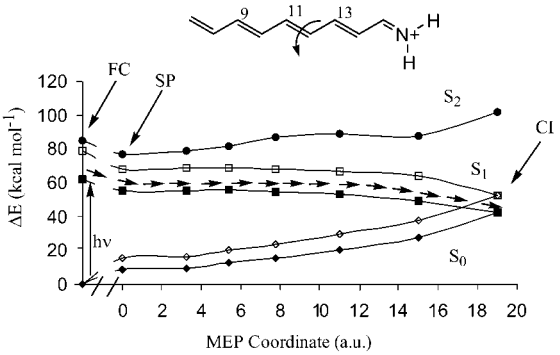

Figure 2. Energy profiles along the S_1 all-trans → 11-cis photoisomerization coordinate of **2**. Full squares indicate the S_1 CASPT2 energies; full circles and diamonds indicate the S_2 and S_0 CASPT2 energies. Open squares and diamonds show the S_1 and S_0 CASSCF energies (i.e., before PT2 correction).

Notice that while there is a considerable correction in the interstate energy gaps when passing from CASSCF to CASPT2, the general shape of the energy profile remains unchanged. In general, the use of CASPT2 to improve the energy accuracy is not recommended in any region where the two states may be highly coupled (i.e., the corresponding wave functions may be mixed), such as in the case of avoided crossings and in the regions surrounding conical intersections. To demonstrate that a conical intersection point located at the CASSCF level remains degenerate after the inclusion of a correction for dynamic correlation, we have carried out MS-CASPT2[23] computations that can, in principle, treat avoided crossings and conical intersections in a balanced way. At a true conical intersection, the coupling is zero, and so the MS-

(14) Kandori, H.; Katsuta, Y.; Ito, M.; Sasabe, H. *J. Am. Chem. Soc.* **1995**, *117*, 2669−2670.
(15) Hou, B.; Friedman, N.; Ruhman, S.; Sheves, M.; Ottolenghi, M. *J. Phys. Chem. B* **2001**, *105*, 7042−7048.
(16) Ye, T.; Friedman, N.; Gat, Y.; H. Atkinson, G.; Sheves, M.; Ottolenghi, M.; Ruhman, S. *J. Phys. Chem. B* **1999**, *103*, 5122−5130.
(17) Zhong, Q.; Ruhman, S.; Ottolenghi, M.; Sheves, M.; Friedman, N.; Atkinson, G. H.; Delaney, J. K. *J. Am. Chem. Soc.* **1996**, *118*, 12828−12829.
(18) Bearpark, M. J.; Robb, M. A.; Schlegel, H. B. *Chem. Phys. Lett.* **1994**, *223*, 269.
(19) Celani, O.; Robb, M. A.; Garavelli, M.; Bernardi, F.; Olivucci, M. *Chem. Phys. Lett.* **1995**, *243*, 1.
(20) Frisch, M. J.; Trucks, G. W.; Schlegel, H. B.; Scuseria, G. E.; Robb, M. A.; Cheeseman, J. R.; Zakrzewski, V. G.; Montgomery, J. A., Jr.; Stratmann, R. E.; Burant, J. C.; Dapprich, S.; Millam, J. M.; Daniels, A. D.; Kudin, K. N.; Strain, M. C.; Farkas, O.; Tomasi, J.; Barone, V.; Cossi, M.; Cammi, R.; Mennucci, B.; Pomelli, C.; Adamo, C.; Clifford, S.; Ochterski, J.; Petersson, G. A.; Ayala, P. Y.; Cui, Q.; Morokuma, K.; Malick, D. K.; Rabuck, A. D.; Raghavachari, K.; Foresman, J. B.; Cioslowski, J.; Ortiz, J. V.; Stefanov, B. B.; Liu, G.; Liashenko, A.; Piskorz, P.; Komaromi, I.; Gomperts, R.; Martin, R. L.; Fox, D. J.; Keith, T.; Al-Laham, M. A.; Peng, C. Y.; Nanayakkara, A.; Gonzalez, C.; Challacombe, M.; Gill, P. M. W.; Johnson, B. G.; Chen, W.; Wong, M. W.; Andres, J. L.; Head-Gordon, M.; Replogle, E. S.; Pople, J. A. *Gaussian 98*, revision A.7; Gaussian, Inc.: Pittsburgh, PA, 1998.
(21) Andersson, K.; Malmqvist, P.-Å.; Roos, B. O. *J. Chem. Phys.* **1992**, *96*, 1218.
(22) Andersson, K.; Blomberg, M. R. A.; Fülscher, M. P.; Karlström, G.; Lundh, R.; Malmqvist, P.-A.; Neogrády, P.; Olsen, J.; Roos, B. O.; Sadlej, A. J.; Schütz, M.; Seijo, L.; Serrano-Andrés, L.; Siegbahn, P. E. M.; Widmark, P.-O. *MOLCAS*, version 4; University of Lund: Lund, Sweden, 1997.
(23) Finley, J.; Malmqvist, P.-Å.; Roos, B. O.; Serrano-Andres, L. *Chem. Phys. Lett.* **1998**, *288*, 299.

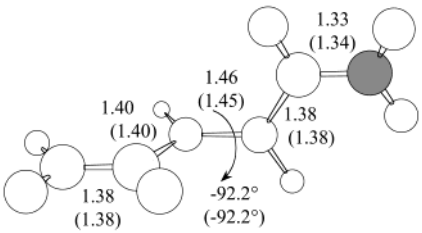

Figure 3. MS-CASPT2 and CASSCF optimized structures of the penta-2,4-dieniminium cation S_1/S_0 conical intersection (geometrical parameters in Å and deg). The MS-CASPT2 geometrical parameters are given in brackets. See Supporting Information for the full sets of Cartesian coordinates.

CASPT2 treatment becomes equivalent to CASPT2 (i.e., the relevant off-diagonal elements of the effective Hamiltonian used in the MS-CASPT2 treatment will be close to zero). The MS-CASPT2 method is, however, very sensitive to the choice of active space, and to obtain correct results it is often necessary to augment an active space with additional virtual orbitals. Because an expanded active space MS-CASPT2 reevaluation of the energy profile of model **2** or, even worse, a MS-CASPT2 reoptimization of the corresponding conical intersection was too expensive to be carried out, we have run a MS-CASPT2 conical intersection optimization[18,24] for the minimal PSB model penta-2,4-dieniminium cation[25] by using a finite difference method developed in our laboratory.[26] In this calculation, the active space comprised six electrons in eight π orbitals.

In Figure 3 we show that, for this minimal model, a true conical intersection exists on the dynamically correlated potential energy surfaces. Comparison of the geometrical parameters of this structure with the corresponding CASSCF structure shows that there are substantially no structural changes. For this reason, in the remaining part of this paper the structure of the CI will be discussed on the basis only of the CASSCF data. The more expensive CASPT2 level of theory will then only be used to determine the energetics of the energy profile in the energy plateau region describing the excited-state barriers.

Given the general flatness of the S_1 energy profile along the computed reaction paths, it is not always technically possible to locate a transition structure at the CASSCF level. Furthermore, even when this is possible, the energy profile recomputed at the CASPT2 level often shows a shifted energy maximum. Thus, throughout the paper the position of the S_1 "transition structures" (TSs) and of the corresponding energy barriers are evaluated as the CASPT2 energy difference between the energy of the SP intermediate and that of the CASPT2 energy profile maximum.

The charge distributions (Mulliken charges) along the model backbones are determined at the CASSCF level of theory. Notice that the charge distribution along the $-C{=}NH_2(+)$ moiety is sensitive to the basis set. For instance, the charge is larger on the N atom when the ANO-S basis set is used but becomes larger on the C atom when the 6-31G* basis is used (see ref 10 for more details). Nevertheless, the charge distribution along the remaining hydrocarbon fragment of the chromophore is basis set independent. In a previous paper[25] on a shorter PSB11 model (i.e., the penta-3,5-dieniminium cation), we demonstrated that, for this system, the atomic charges computed using different schemes (NPA, CHelpG, MKS) yield the same distribution. Similarly, the computed *total* natural bond orbital (NBO)[27] charges give, again, the same type of distribution.

The investigation of the structure of the S_1 and S_0 potential energy surfaces in the vicinity of the CI points associated with the different excited-state paths has been carried out for **2** by scanning along a molecular displacement corresponding to double bond expansion − single bond contraction (see section 3.5 below) by applying a step of −0.005 and +0.005 Å to each single and double bond, respectively. The shape of the S_0 surface structure in this region has been further characterized by standard transition structure optimization.

3. Results and Discussion

The energies of the intermediates, transition structures, and conical intersections discussed below are collected in Table 1. The corresponding structures are given in the Supporting Information. The S_0, S_1, and S_2 energy profiles computed along the 11-cis → all-trans and all-trans → 11-cis isomerization coordinates for **1** and **2**, respectively (see Figures 1 and 2), indicate that the S_2 energy profile is always more than 20.0 kcal mol^{-1} higher in energy than the S_1 state. All models considered in this paper show this behavior. Thus, as previously reported,[10] PSB photoisomerization involves two electronic states. In the following, we shall therefore limit ourselves to a discussion of the structure of the S_1 and S_0 energy profiles as well as of the S_1/S_0 conical intersection region. All computed reaction paths start at the optimized relaxed S_1 planar intermediate SP.

3.1. Free Chromophores. In Figure 4 we compare the energy profiles associated with the reaction coordinates of the PSBT model **2** leading toward the 9-cis, 11-cis, and 13-cis forms (i.e., structures **4**, **demethyl-1**, and **3**, respectively). There are three general features: (i) In all cases, the S_1 energy profiles display a flat plateau (i.e., with a barrier less than 3.0 kcal mol^{-1}) that develops from the planar SP point to a significantly twisted structure. The energy plateau ends after ca. 40° twisting along the all-trans → 11-cis coordinate, at ca. 50° along the all-trans → 13-cis coordinate, and persists all along the all-trans → 9-cis coordinate. (ii) The S_1 energy barriers are (in ascending order) all-trans → 11-cis (0.2 kcal mol^{-1}), all-trans → 13-cis (0.5 kcal mol^{-1}), and all-trans → 9-cis (3.0 kcal mol^{-1}). (iii) In all cases, the energy profile ends at a ca. 90° twisted structure. However, while the all-trans → 11-cis reaction coordinate ends at a S_1/S_0 intersection CI, both the all-trans → 13-cis and all-trans → 9-cis paths first lead to a ca. 90° twisted energy minimum (TM) on the S_1 surface. As previously demonstrated by Martinez, Ben-Nun et al. for the all-trans → 13-cis case,[28] these minima are located near two CIs (not reported in Figure 4) that are entered via a displacement along a single bond contraction−double bond expansion stretching mode. These CIs lie at a slightly higher energy than the minima (ca. 2.5 kcal mol^{-1} in our computation; see ref 29), and their relationship to the corresponding TMs will be discussed in section 3.5. (iv) The change in S_1 and S_0 charge distribution computed along the all-trans → 11-cis path is shown in Figure 5. Notice that, as previously reported for **1**,[10] upon $S_0 \rightarrow S_1$ excitation the maximum of the positive charge distribution moves from the N-end toward the C-end of the

(24) Ragazos, I. N.; Robb, M. A.; Bernardi, F.; Olivucci, M. *Chem. Phys. Lett.* **1992**, *197*, 217.
(25) Garavelli, M.; Celani, P.; Bernardi, F.; Robb, M. A.; Olivucci, M. *J. Am. Chem. Soc.* **1997**, *119*, 6891−6901.
(26) Geometry optimizations at the multistate CASPT2/6-31G* level were carried out using a numerical gradient code developed by the authors for use with Molcas 4.1. Cartesian displacements of 0.001 Å were used, along with the gradient generated by finite differences. In this work, a π-valence active space was selected, comprising six electrons in eight orbitals. Full details are given in: Page, C. S.; Olivucci, M. *J. Comput. Chem.* **2002**, submitted for publication.
(27) Reed, A. E.; A. Curtiss, L.; Weinhold, F. *Chem. Rev.* **1988**, *88*, 899−926.
(28) Molnar, F.; Ben-Nun, M.; Martinez, T. J.; Schulten, K. *J. Mol. Struct.* **2000**, *506*, 169−178.
(29) This CI has been located via a two-dimensional scan carried out at the CASSCF level of theory. The corresponding grid has been computed by applying a step of +0.02 Å and −0.02 Å to the C−C bond and C−N bond of the $-CH-CH-NH_2$ moiety, respectively. See the Supporting Information for the raw data.

Table 1. CASSCF/6-31G* Absolute and CASPT2/6-31G* Absolute and Relative Energies of the Structures Discussed in the Text[a]

structure	state	CASSCF energy (hartree)[b]	CASPT2 energy (hartree)[b]	relative energy CASPT2 level (kcal mol^{-1})[c]
		all-*trans*-nona-2,4,6,8-tetraeniminium cation model **2**		
FC	S_0	−402.0934	−403.3242 [0.72]	−55.5
	S_1	−401.9674	−403.2252 [0.70]	6.6
	S_2		−403.1888 [0.70]	29.5
SP	S_0	−402.0691	−403.3104 [0.71]	−46.8
	S_1	−401.9845	−403.2358 [0.70]	0.0
	S_2		−403.2014 [0.70]	21.6
TS (all-trans → 9-cis)	S_0	−402.0238	−403.2724 [0.71]	−23.0
	S_1	−401.9791	−403.2310 [0.70]	3.0
TM (all-trans → 9-cis)	S_0	−401.9986		
	S_1	−401.9889		
CI (all-trans → 9-cis)	S_0	−401.9809		
	S_1	−401.9786		
TS (all-trans → 11-cis)	S_0	−402.0609	−403.3039 [0.71]	−42.7
	S_1	−401.9835	−403.2354 [0.70]	0.2
	S_2		−403.1938 [0.69]	26.4
CI (all-trans → 11-cis)	S_0	−402.0100	−403.2561 [0.71]	−12.7
	S_1	−402.0091	−403.2563 [0.70]	−12.9
	S_2		−403.1620 [0.68]	46.3
TS_1 (ground-state all-trans → 11-cis)	S_0	−402.0139		
	S_1	−402.0018		
TS_2 (ground-state all-trans → 11-cis)	S_0	−402.0150		
	S_1	−402.0005		
TS (all-trans → 13-cis)	S_0	−402.0630	−403.3055 [0.71]	−43.7
	S_1	−401.9829	−403.2350 [0.70]	0.5
TM (all-trans → 13-cis)	S_0	−402.0142		
	S_1	−402.0002		
CI (all-trans → 13-cis)	S_0	−401.9975[d]		
	S_1	−401.9961[d]		
TS_3 (ground-state all-trans → 13-cis)	S_0	−402.0268		
	S_1	−401.9910		
		13-cis-nona-2,4,6,8-tetraeniminium cation model **3**		
FC	S_0	−402.0878	−403.3189 [0.72]	−55.1
	S_1	−401.9642	−403.2215 [0.70]	6.0
SP	S_0	−402.0634	−403.3051 [0.71]	−46.4
	S_1	−401.9796	−403.2311 [0.70]	0.0
TM (13-cis → all-trans)	S_0	−402.0143		
	S_1	−401.9999		
CI (13-cis → 11-cis, 13-cis)	S_0	−402.0028		
	S_1	−402.0016		
		9-cis-nona-2,4,6,8-tetraeniminium cation model **4**		
FC	S_0	−402.0896	−403.3204 [0.72]	−56.0
	S_1	−401.9632	−403.2214 [0.70]	6.1
SP	S_0	−402.0646	−403.3063 [0.71]	−47.1
	S_1	−401.9798	−403.2312 [0.70]	0.0
TM (9-cis → all-trans)	S_0	−402.0006		
	S_1	−401.9887		
		3-penta-2,4-dienylidene-cyclopent-1-enylmethyliminium cation model **2-locked**		
FC	S_0	−479.0027	−480.5054 [0.67]	−51.3
	S_1	−478.8798	−480.4123 [0.66]	7.2
SP	S_0	−478.9782	−480.4932 [0.67]	−43.6
	S_1	−478.8972	−480.4237 [0.66]	0.0
CI (all-trans → 11-cis)	S_0	−478.9203		
	S_1	−478.9199		
		2-hexa-1,3,5-trienyl-cyclopent-1-enylmethyliminium cation model **3-locked**		
FC	S_0	−518.0389	−519.6777 [0.65]	−52.8
	S_1	−517.9112	−519.5818 [0.63]	7.3
SP	S_0	−518.0095	−519.6618 [0.65]	−42.8
	S_1	−517.9286	−519.5935 [0.64]	0.0
TS (13-cis → 11-cis, 13-cis)	S_0	−518.0089	−519.6593 [0.65]	−41.3
	S_1	−517.9282	−519.5915 [0.64]	1.2
CI (13-cis → 11-cis, 13-cis)	S_0	−517.9522		
	S_1	−517.9514		
		2-(4-allylidene-cyclopent-2-enylidene)-ethyliminium cation model **1-locked**		
FC	S_0	−439.9671	−441.3345 [0.69]	−54.1
	S_1	−439.8462	−441.2406 [0.68]	4.8
SP	S_0	−439.9617	−441.3344 [0.69]	−54.0
	S_1	−439.8556	−441.2483 [0.68]	0.0
TS (11-cis → 11-cis, 13-cis)	S_0	−439.9361	−441.3213 [0.69]	−45.8
	S_1	−439.8542	−441.2450 [0.67]	2.1
TM (11-cis → 11-cis, 13-cis)	S_0	−439.8968		
	S_1	−439.8727		

[a] The weights of the zeroth order wave function in the CASPT2 wave function are given in square brackets. [b] Minimum energy paths have been calculated with two roots state average CASSCF wave functions (energies given). At selected geometries, three roots state average CASSCF wave functions were calculated (energies not shown); these represented the zeroth order wave functions for the CASPT2 results quoted (see also Computational Details). [c] For each model, energies are relative to the S_1 state energy of the SP structure. [d] Energies taken from Tables 2 and 3 in the Supporting Information and relative to point (C−C 1.49 Å, C−N 1.26 Å). See also ref 29.

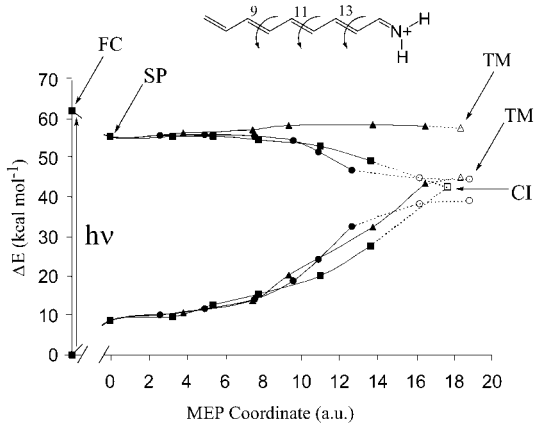

Figure 4. CASPT2 energy profiles along the S_1 all-trans → 9-cis (full triangles), all-trans → 11-cis (full squares), and all-trans → 13-cis (full circles) photoisomerization coordinates of **2**. Open triangles, open squares, and open circles indicate the corresponding CASSCF energy profiles in the regions where the S_1-S_0 energy gap is less than 10 kcal mol^{-1}. These comprise the ca. 90° twisted S_1 energy minimum TM (for the all-trans → 9-cis and all-trans → 13-cis paths) and the S_1/S_0 conical intersection CI (for the all-trans → 11-cis path).

chromophore. Furthermore, the charge shift is augmented upon torsional deformation and results in a full charge transfer at the 90° twisted CI (all-trans → 11-cis) and minima TM (all-trans → 13-cis and all-trans → 9-cis). This behavior is common to all investigated paths and models. As such, we do not discuss this issue for the additional cases discussed below.

In Figure 6 we compare the energy profiles associated with the reaction coordinates of the PSB13 model **3** and PSB9 model **4**. For **3** we have computed two different paths. The 13-cis → all-trans path of Figure 6a corresponds, with respect to the all-trans → 13-cis path of Figure 4, to a reverse photoisomerization. In contrast, the energy profile of Figure 6b corresponds to the 13-cis → 11-cis, 13-cis process leading to a "double-cis" stereoisomer. Both paths are substantially barrierless (i.e., less than ca. 1.0 kcal mol^{-1}) with a larger slope for the 13-cis → all-trans case. Finally, in Figure 6c we show the energy profile corresponding to the 9-cis → all-trans photoisomerization. Again, this process corresponds to a reverse reaction (i.e., with respect to the all-trans → 9-cis path of Figure 4). However, in contrast to the direct process, the computed energy barrier is only 0.1 kcal mol^{-1}, and so the reaction is effectively barrierless.

3.2. Locked Chromophores. In Figure 7a we report the photoisomerization path for the all-trans PSB13.5 model **2-locked**. This path must be compared with the corresponding all-trans → 11-cis path of Figure 4. It is evident from the figure that the presence of the lock does not alter the general behavior described for the free chromophore and the reaction path is barrierless. This indicates that, in **2-locked**, the presence of the lock in a position adjacent to the reactive double bond does not lead to stabilization of the SP structure. Furthermore, as with the free chromophore, the path ends at a ca. 90° twisted S_1/S_0 CI. In Figure 7b we report the photoisomerization energy profile of model **3-locked**. This second type of lock (i.e., the five-membered ring lock now comprises two rather than three atoms of the conjugated chain) shows a similar behavior. In fact, the computed 13-cis-locked → 11-cis, 13-cis-locked path is again substantially barrierless.

In Figure 7c we show the behavior of model **1-locked** with respect to the 11-cis-locked → 11-cis-locked, 13-cis process. Similar to the cases of **2-locked** and **3-locked**, the lock (which is structurally different from the previous two since it comprises four rather than two or three atoms of the conjugated chain) is expected to have a limited effect on the reaction energy profile about adjacent unlocked double bonds. However, for this chromophore, we compute a substantial S_1 barrier for the isomerization of both the double bond in position 13 and the double bond in position 9. Indeed, the 11-cis-locked → 9-cis, 11-cis-locked process has a 5.0 kcal mol^{-1} barrier, and the 11-cis-locked → 11-cis-locked, 13-cis process of Figure 7c has a 2.0 kcal mol^{-1} barrier. Because of the absence of a barrierless path, the planar SP intermediate of **1-locked** must have the longer excited-state lifetime among the PSBs.

3.3. Correlation between Computed and Experimental Results. The photoinduced dynamics of both native and locked PSBs in methanol solution have been investigated by means of time-resolved spectroscopic methods. These experiments have provided a measure of the S_1 excited-state lifetime and, in turn, of the effect of the lock on the S_1 decay rate. Below we show that the observed changes in lifetime correlate with the changes in the magnitude of the barrier located along the S_1 paths discussed in the previous sections.

Both S_1 all-trans and 11-cis PSBs have a 2−3 ps S_1 lifetime.[14,30] This lifetime is associated with the time scale required for S_1 vibrational energy redistribution and evolution along the *barrierless* energy plateau of the all-trans → 11-cis (see Figure 2) and 11-cis → all-trans (see Figure 1) paths, respectively. In fact, as discussed above for **1**, the bimodal nature of the excited-state reaction coordinate implies that, immediately after the initial FC → SP relaxation, the vibrational energy is located on totally symmetric stretching modes. This energy must thus be redistributed before evolution along the weakly coupled asymmetric SP → CI torsional coordinate (ultimately leading to $S_1 \rightarrow S_0$ decay) begins. Notice that for model **1** the retinal methyl group in position 13 has been preserved to describe the steric interaction with the hydrogen in position 10 that contributes to 11-cis → all-trans torsional destabilization of PSB11 (this destabilization contributes to speed up the 11-cis → all-trans motion in rhodopsin[31]). The all-trans → 11-cis path of Figure 2 indicates that such steric interaction is not a prerequisite for barrierless isomerization about the double bond in position 11.

The all-trans PSB13.5 and 11-cis PSB11.5 chromophores provide two cases where the effect of the lock on the excited-state time scale can be probed. In fact, according to the results presented in Figures 4 and 7c for **2-locked** and **1-locked**, one can predict distinct behaviors for these two PSB chromophores. In particular, upon locking of all-trans PSB a barrierless all-trans → 11-cis path remains operative, and one would not predict a significant change in excited-state lifetime. In contrast, upon locking of 11-cis PSB, no barrierless isomerization path remains operative, and the most favorable path shows a 2.0 kcal mol^{-1} energy barrier. As a consequence, a marked increase in excited-state lifetime is predicted. Consistent with these predictions, the measured lifetimes of all-trans PSB13.5 and 11-cis PSB11.5 in methanol solution are 2−3 ps[15] and 19 ps,[14] respectively. It is

(30) Lugonov, S. L.; Song, L.; El-Sayed, M. A. *J. Phys. Chem.* **1996**, *100*, 18586−18591.
(31) Wang, Q.; Kochendoerfer, G. G.; Schoenlein, R. W.; Verdegem, P. J. E.; Lugtenburg, J.; Mathies, R. A.; Shank, C. V. *J. Phys. Chem.* **1996**, *100*, 17388−17394.

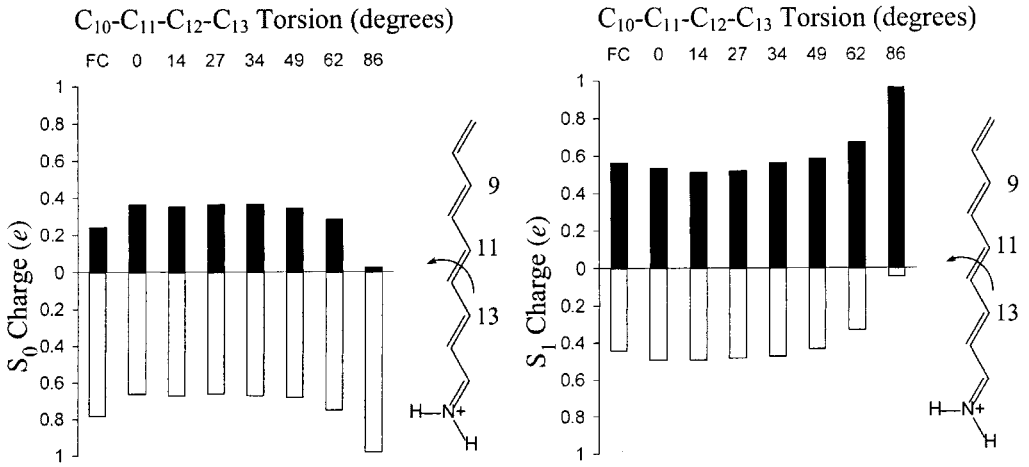

Figure 5. Distribution of the CASSCF Mulliken charges along the all-trans → 11-cis photoisomerization path of **2**. The bar diagrams give the S_0 (left diagram) and S_1 (right diagram) charges for the $H_2C{=}CH{-}CH{=}CH{-}CH$ (top) and $CH{-}CH{=}CH{-}CH{=}NH_2$ (bottom) moieties.

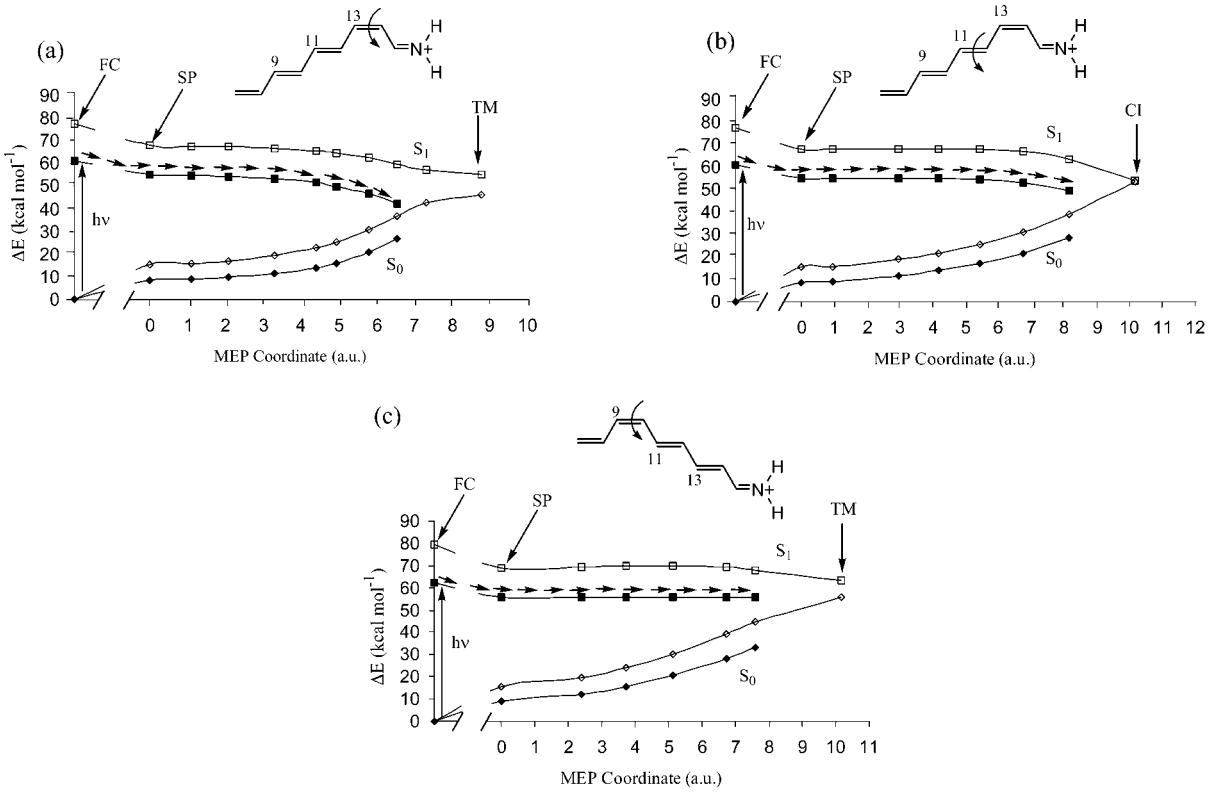

Figure 6. Energy profiles along (a) the S_1 13-cis → all-trans, photoisomerization coordinate of **3**, (b) the 13-cis → 11-cis, 13-cis photoisomerization coordinate of the same model, and (c) the S_1 9-cis → all-trans photoisomerization coordinate of **4**. Full squares indicate the CASPT2 S_1 energies; full diamonds show the CASPT2 S_0 energies. Open squares and diamonds show the S_1 and S_0 CASSCF energies (i.e., before PT2 correction).

therefore apparent that the results of our calculations correlate qualitatively with the experiment. Further evidence for this correlation comes from the observed excited-state lifetime of the 13-cis locked chromophore 13-cis PSB13.5. In fact, similarly to all-trans PSB13.5, this chromophore decays in 2−3 ps indicating that a substantially barrierless isomerization path is still operative in the locked molecule.[15] Indeed, as reported in Figure 6b for the 13-cis PSB13.5 model **3-locked**, the path corresponding to the isomerization of the double bond in position 11 is essentially barrierless.

3.4. Photoisomerization of Locked Chromophores in Rhodopsin and Bacteriorhodopsin. The correlation between the computed S_1 energy profiles and observed S_1 lifetimes also provides *indirect* information on the effect of the protein cavity on the potential energy surface of the PSB chromophores. For instance, in bacteriorhodopsin the excited-state lifetime of all-trans PSB is reduced from 2 to 3 ps to 0.2 ps.[16,17] Furthermore, in contrast to the solution environment where the all-trans → 11-cis motion prevails, the isomerization corresponds to an all-trans → 13-cis stereospecific process. The reduced excited-state lifetime suggests that in the protein the all-trans → 13-cis energy profile of Figure 4 becomes favored. In other words, the long energy plateau is greatly reduced or even removed. On the other hand, it is not clear if the protein acts exclusively by "catalyzing" the all-trans → 13-cis route or if it also inhibits the favored all-trans → 11-cis path as suggested by the stereospecificity.

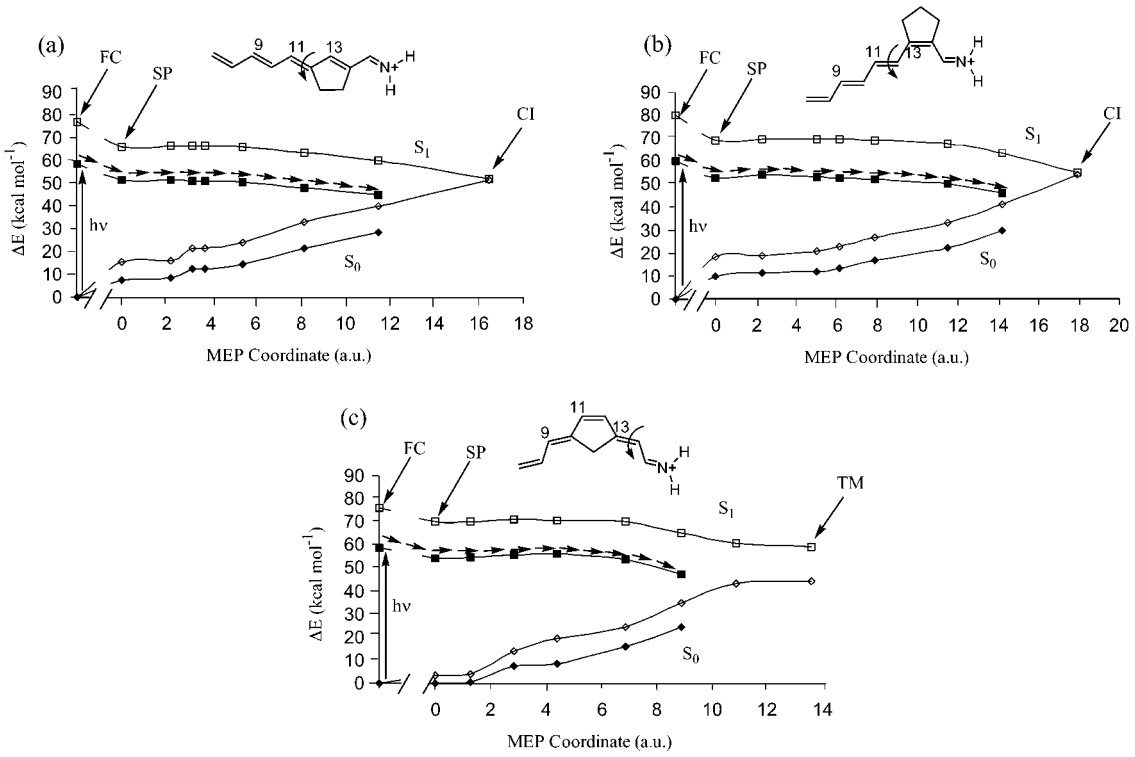

Figure 7. Energy profiles along (a) the S_1 all-trans → 11-cis, photoisomerization coordinate of **2-locked**, (b) the 13-cis → 11-cis, 13-cis photoisomerization coordinate of **3-locked**, (c) the S_1 11-cis → 11-cis, 13-cis photoisomerization coordinate of **1-locked**. Full squares and full diamonds indicate the CASPT2 S_1 and S_0 energies along the same coordinate, respectively. Open squares and diamonds show the S_1 and S_0 CASSCF energies (i.e., before PT2 correction).

The results of a recent spectroscopic investigation[16,17] of an artificial bacteriorhodopsin containing the all-trans PSB13.5 chromophore have revealed that upon locking, the excited-state lifetime of the protein undergoes a ca. 10-fold increase up to ca. 20 ps. This behavior is substantially different from that of the corresponding locked chromophore in solution where the lock does not change the lifetime.[15] Thus, the locked bacteriorhodpsin lifetime increase suggests that the all-trans → 11-cis energy profile is destabilized by the protein cavity in such a way that a few kcal mol^{-1} barrier impairs the access to the conical intersection. Our models would then suggest that photoisomerization in bacteriorhodopsin is the result of simultaneous specific "catalysis" (all-trans → 13-cis path) accompanied by specific "inhibition" (all-trans → 11-cis path).

The above model must also be valid for rhodopsin. In this case, the protein environment catalyzes the 11-cis → all-trans path making it more attractive (and also coupling the stretching and the torsional modes to speed up vibrational energy redistribution). Again, in the artificial protein containing the 11-cis PSB11.5 locked chromophore, the observed lifetime is ca. 4 times longer (ca. 85 ps) than the lifetime of the corresponding locked chromophore in solution.[14] This suggests that, in rhodopsin, the protein cavity, which specifically catalyzes the 11-cis → all-trans, also "inhibits" the alternative 11-cis →11-cis, 13-cis motion.

The reaction paths of Figure 7b and c support the idea that the 13-cis PSB13.5 and 11-cis PSB11.5 locked chromophores could undergo trans to cis photoisomerization at positions 11 and 13, respectively. While the observable production of the resulting di-cis locked retinals may be limited by an unfavorable branching at the corresponding conical intersection, careful experimental work on the solution photochemistry of 13-cis PSB13.5 and 11-cis PSB11.5 would be important as a test of the mechanistic view proposed above. Indeed, while production of di-cis retinals has not been observed during photolysis of a 11-cis PSB11.5 in rhodopsin,[32] irradiation of a *six-membered* ring 11-cis locked PSB in rhodopsin afforded 11,13 and 11,9 di-cis photoproducts.[33]

3.5. Structure of the Conical Intersection Regions. While the S_1 lifetimes must depend exclusively on the evolution of the chromophore along its S_1 potential energy surface, this is not the case for the photoisomerization quantum yields. Indeed, the relative population of the all-trans → 9-cis, all-trans → 11-cis, all-trans → 13-cis, etc. paths is only one factor which contributes to determine the final quantum yield distribution. A second critical factor is the unavoidable path branching occurring upon $S_1 \rightarrow S_0$ decay at the corresponding conical intersections. This branching reflects the wave packet motion in the region of the conical intersection. In principle, only semiclassical or quantum dynamics methodologies can provide a rigorous answer to this problem. However, very regrettably, the application of these methodologies to realistic (accurate) multidimensional potential energy surfaces of **1** and **2** is still substantially out of reach.

The results of trajectory and wave packet calculations depend critically on the shape of the S_1 and S_0 potential energy surfaces in the region close to the conical intersection. For this reason, in this section we present a characterization of the shape of the S_1 surface associated with the all-trans → 11-cis, all-trans → 13-cis CIs. As shown above, the all-trans → 13-cis pathway

(32) Ito, M.; Katsuta, Y.; Imamoto, Y.; Shichida, Y.; Yoshizawa, T. *Photochem. Photobiol.* **1992**, *56*, 915−919.
(33) Jang, G.-F.; Kuksa, V.; Filipek, S.; Bartl, F.; Ritter, E.; Gelb, M. H.; Hofmann, K. P.; Palczewski, K. *J. Biol. Chem.* **2001**, *276*, 26148−26153.

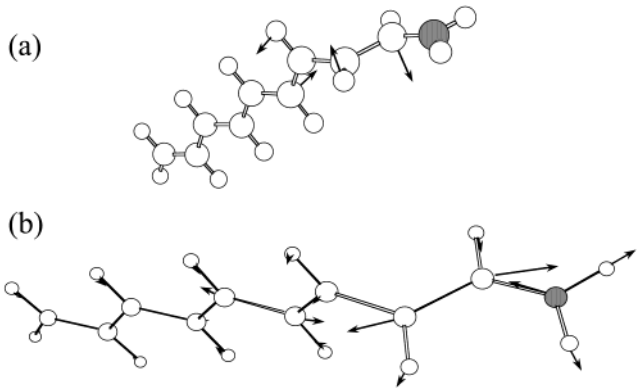

Figure 8. Branching plane vectors for the CI of **2** along the all-trans → 13-cis photoisomerization coordinate. (a) Nonadiabatic coupling vector and (b) gradient difference vector.

does not lead directly to a conical intersection but to an energy minimum TM displaying a ca. 90° twisted double bond in position 13. In agreement with previous studies,[28] we have found that a CI point located slightly *above* the minimum can be entered by progression along a mode dominated by a double bond expansion−single bond contraction of the N-containing moiety.[29] This stretching mode is nearly orthogonal to the SP → TM coordinate characterized by a 90° torsion change and nearly parallel to one of the vectors defining the conical intersection branching plane.[34] This mode (the gradient difference vector) is shown in Figure 8b and corresponds to a single bond contraction−double bond expansion mode localized exclusively along the N-containing moiety of **2**. The same features are found for the all-trans → 9-cis process.

To gain insight into the mechanism of the $S_1 \rightarrow S_0$ decay process, it is of interest to clarify the relationship between the shapes of the S_1 and S_0 energy surfaces in the CI region. This has been accomplished by carrying out, for both the all-trans → 11-cis and all-trans → 13-cis CIs of **2**, a one-dimensional scan of the CASSCF energy surfaces along the direction of the branching plane mode discussed above (see section 2 for details). The results of the scan are given in Figure 9.

The first general feature of the shape of the S_0 energy surface in these regions is that it contains the transition structures for the *thermal* cis−trans isomerization. In fact, in the case of the conical intersection associated to the all-trans → 11-cis process, we could locate, on opposite sides of the cone tip, two different S_0 minima (see Figure 9a). This finding indicates the energy surface shape given in Scheme 1a where the minima correspond to the distinct S_0 transition structures TS_1 and TS_2, and the conical intersection is "peaked".[34] Thus, the scanning coordinate defines a $TS_1 \rightarrow CI \rightarrow TS_2$ S_0 energy ridge that divides the S_0 reactant (trans) and product (cis) valleys. Consistent with the general theory of conical intersections,[35] the electronic structures of the two minima are found to be different and can be described as an in-phase and an out-of-phase mixture of the S_0 and S_1 wave functions discussed in section 3.1. This confirms that, as expected, the electronic structure of the energy surface is a rapidly changing function of the nuclear coordinates in the conical intersection region. In Figure 9b we show that, for the alternative case of the conical intersection associated to the all-

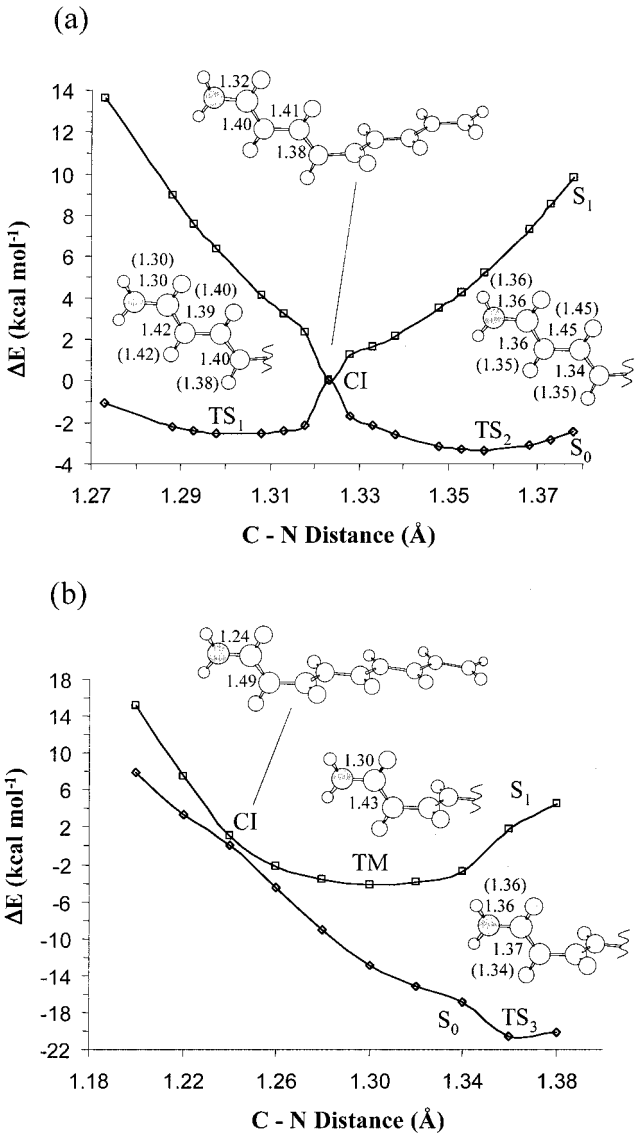

Figure 9. CASSCF energy profiles along a double bond expansion−single bond contraction mode defined in section 2 for (a) the CI point of the all-trans → 11-cis path of **2** and (b) the TM point of the all-trans → 13-cis path of **2**. The geometrical parameters of the optimized transition state structures (TS_1, TS_2, TS_3) are given in brackets (values in Å). The CI located in (b) is ca. 4.8 kcal mol^{-1} higher in energy then the TM; this is due to the less comprehensive monodimensional scan performed in this case. See also ref 29.

trans → 13-cis process, the computed energy profile shows only one S_0 energy minimum. This finding suggests an energy surface shape of the type illustrated in Scheme 1b where the minimum corresponds to a transition structure TS_3, and the conical intersection is "sloped".[34] Notice that the S_1 90° twisted energy minimum TM is located in the region above the S_0 TS_3 structure. Thus, these two points differ in electronic structure and are related by an intramolecular charge transfer. Indeed, while in the S_1 minimum the positive charge is located in the N-containing hydrocarbon moiety, in TS_3 the positive charge is located in the other moiety (see also section 3.1). Evidence in favor of the potential energy surface topologies of Scheme 1a and b has been produced by rigorous S_0 transition state searches in the full space of the nuclear degrees of freedom of the system. Three transition structures have indeed been located in the strict

(34) Atchity, G. J.; Xantheas, S. S.; Ruedenberg, K. *J. Chem. Phys.* **1991**, *95*, 1862−1876.
(35) Bernardi, F.; Olivucci, M.; Robb, M. A. *Chem. Soc. Rev.* **1996**, 321−328.

Scheme 1

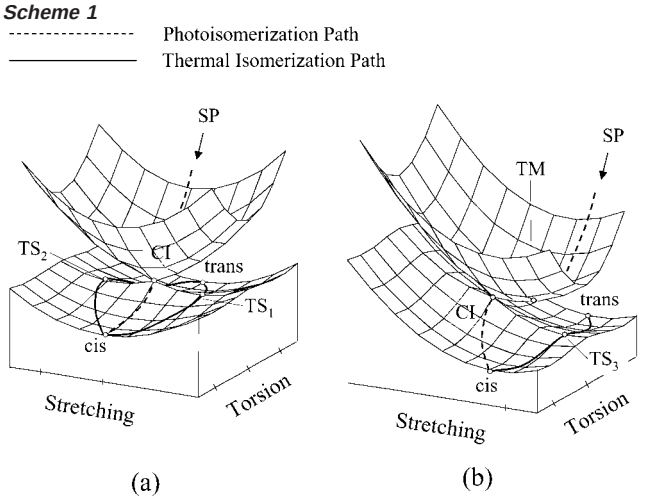

vicinity of the S_0 energy minima of Figure 9. Their relevant geometrical parameters are given in the same figure.

Making the assumption that the excited-state trajectories will follow, in the average, the computed excited-state paths of Figure 4, a qualitative difference between the all-trans → 11-cis and all-trans → 13-cis (and 9-cis) cases is immediately apparent. In the first case, the trajectories will enter the conical intersection directly, while in the second case, the trajectories must undergo a number of oscillations (in a direction orthogonal to the torsional motion) in the region of TM before entering the CI. Thus, as suggested by Martinez, Ben-Nun et al.,[36] the different topologies may be related to different quantum yields for the 11-cis and 13-cis products. On the other hand, one should notice that the local $-CH-CH-NH_2$ stretching mode connecting TM to CI (see Figure 10a) for the case of the all-trans → 13-cis has the same direction (but opposite sign) of the extended stretching mode describing the initial FC → SP relaxation motion (see Figure 10b). As a consequence, one may expect that, given the barrierless nature of the SP → TM reaction coordinate (and thus the inefficient vibrational energy redistribution at SP), the retinal molecule will arrive at TM with a considerable vibrational excess energy located along the TM → CI mode, so making the decay faster and the TM lifetime much shorter. Notice also that for **2** a significant stretching component is still present during the SP → TM deformation. This seems not to be the case for the all-trans → 11-cis path (or the 11-cis → all-trans path of model **1**), where a twisted minimum does not exist.

In conclusion, there are at least two factors determining the quantum yield of the all-trans → 11-cis process with respect to the all-trans → 13-cis process. The first is related to the structure of the different competitive excited-state paths that leads to a different population of the competitive isomerization paths. In this respect, one would predict a similar population for the all-trans → 11-cis and all-trans → 13-cis paths since these are both barrierless. The second factor is related to the reactant/product branching occurring upon decay at the funnel. According to this factor, the first process shall be favored with respect to the second. The all-trans → 9-cis process is predicted to be disfavored by both factors. This model provides a qualitative rationalization of the quantum yields observed for PSBs in methanol solution.[8] Indeed, the 11-cis > 13-cis > 9-cis photoproduct ratio observed for the photolysis of PSBT is readily explained. The results of the photolysis of PSB11 permit a similar explanation since the only detected photoproduct is PSBT, thus demonstrating prevailing 11-cis → all-trans motion. On the other hand, neither of the two factors discussed above seems to be able to explain the observed low *total* (ca. 0.25) quantum yield observed for both PSBT and PSB11 photoisomerization. Indeed, these data strongly suggest that at least 50% of the excited-state molecules never reach the conical intersection funnel but are quickly returned to the S_0 reactant valley. The factor (either structural or dynamical) that accounts for this reduction in total quantum yield is presently unknown and is a matter of current research in our laboratory.

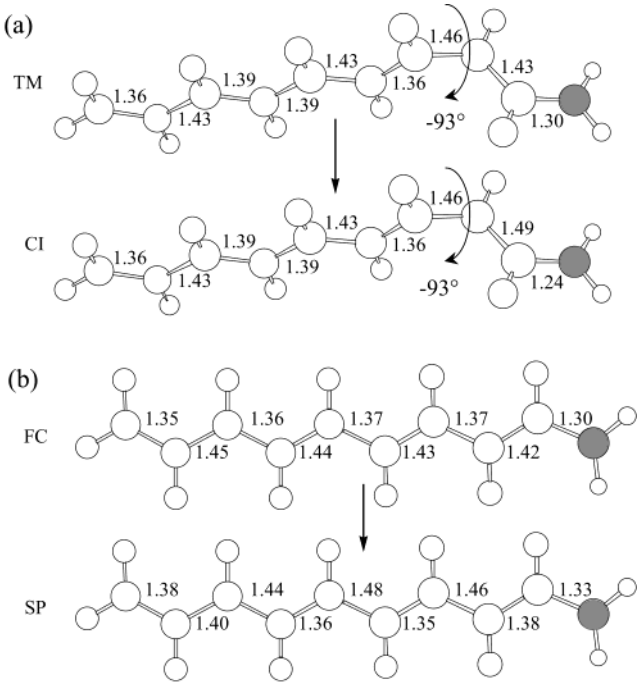

Figure 10. (a) TM and CI molecular structures relative to the all-trans → 13-cis path of **2**. The relevant geometrical parameters are given in Å and deg. (b) FC and SP molecular structures of **2**.

4. Conclusions

Reaction path mapping for the retinal protonated Schiff base models **2** and **3** provides quantitative evidence that retinal chromophores are tunable photochemical systems. In fact, the presence of three competitive photoisomerization paths (the differences in barriers are within 0.0−3.0 kcal mol^{-1}) indicates that even a moderate stabilization of a specific route and/or a destabilization of the alternative routes (for instance in the protein cavity) will make the reaction fully stereospecific. Thus, our computations provide a rational basis for understanding the photoisomerization selectivity in rhodopsin, bacteriorhodopsin, dark-adapted bacteriorhodopsin, and isorhodopsin where the 11-cis, 13-trans, 13-cis, and 9-cis bonds are isomerized, respectively.

We have shown that "locking" one photoisomerization path in an artificial chromophore where a double bond is embedded in a five-membered ring does not necessarily change the order of magnitude of the excited-state lifetime. Our results on **2-locked** demonstrate that the presence of a 13.5 lock compris-

(36) Ben-Nun, M.; Molnar, F.; Schulten, K.; Martinez, T. J. *Proc. Natl. Acad. Sci. U.S.A.* **2002**, *99*, 1769−1773.

ing three atoms of the retinal chain does not appreciably change the S_1 energy profile for the isomerization of the double bond in position 11. Similarly, a 13.5 lock comprising two atoms of the chain as in **3-locked** does not significantly affect the stability of the S_1 path for the same isomerization. On the other hand, we have seen that a 11.5 lock comprising four carbon atoms of the chain (necessarily a cis chain), as in **1-locked**, leads to creation of a significant excited-state barrier for the isomerization about the double bond in position 13 with a consequent increase in lifetime. Remarkably, the use of locks of different sizes, such as six-, seven-, and eight-membered rings, leads to different, sometimes surprising, S_1 lifetime changes. In particular, it has been experimentally demonstrated[37,38] that an eight-membered ring lock decreases the excited-state lifetime. The "catalytic" effect of this ring is currently under investigation in our laboratory.

Finally, an analysis of the structures of the S_1 and S_0 surfaces at the bottom of the all-trans → 9-cis, all-trans → 11-cis, and all-trans → 13-cis paths of **2** has shown that the conical intersection which mediates the isomerization about the double bond in position 11 has a peaked topology. In contrast, the paths for the isomerization about the adjacent double bonds in positions 9 and 13 involve conical intersections with sloped topologies.

Acknowledgment. We are grateful to Profs. M. Ottolenghi, S. Ruhman, and M. Merchán for helpful discussions. Funds have been provided by the Università di Siena (Progetto di Ateneo A.A. 00/02), NATO (CRG 950748), and HFSP (RG 0229/2000-M). C.S.P. and M.O. are grateful for the EU Marie-Curie Grant No. HPMF-CT-1999-00384. We wish to thank the "Swiss Center for Scientific Computing" and "Cineca" for granted calculation time on their computers.

Supporting Information Available: Cartesian coordinates of all structures discussed in the text, and three tables (Tables 2−4) containing the S_0, S_1, S_1-S_0 energies relative to the two-dimensional scan defined in ref 29 (PDF). This material is available free of charge via the Internet at http://pubs.acs.org.

JA017502C

(37) Kandori, H.; Matuoka, S.; Shichida, Y.; Yoshizawa, T.; Ito, M.; Tsukida, K.; Balogh-Nair, V.; Nakanishi, K. *Biochemistry* **1989**, *28*, 6460−6467.

(38) Kandori, H.; Sasabe, H.; Nakanishi, K.; Yoshizawa, T.; Mizukami, T.; Shichida, Y. *J. Am. Chem. Soc.* **1996**, *118*, 1002−1005.